RSC Advances

ROYAL SOCIETY OF CHEMISTRY

www.rsc.org/advances

Cite this: DOI: 10.1039/c0xx00000x

www.rsc.org/xxxxxx

ARTICLE TYPE

A Facile Interfacial Assembling Strategy for Synthesizing Yellow TiO_2 Flakes with a Narrowed Bandgap

Jingyu Wang,*[a] Yizhi Zhao,[b] Xiaochan Xu,[a] Xiaoli Feng,[a] Junxia Yu[c] and Tao Li*[a]

Received (in XXX, XXX) Xth XXXXXXXXX 20XX, Accepted Xth XXXXXXXXX 20XX

DOI: 10.1039/b000000x

As a promising photocatalyst, the large bandgap (3.2 eV) of anatase TiO_2 seriously limits its light absorption to UV portion of solar spectrum, making it less applicable in industrial fields. A popular approach for enhancing visible light activity by narrowing the bandgap is doping, however, the dopant-induced defect states in the TiO_2 lattice may act as recombination centers for the photogenerated charge carriers. Here we report a facile soft-chemical route to engineer the surface properties of TiO_2 crystals using ethanol as the sole organic solvent. The individual TiO_2 nanocrystals synthesized in the first step, possessing high affinity with ethanol molecules, tend to assemble together by interfacial Ti-Ti bonding during the followed ethanol evaporation induced self-assembly process. Formation of Ti-Ti bonds at the interface simultaneously brings about the decrease of surface oxygen atom in TiO_2 structural unit, which dramatically alters the electronic structure and extends the light absorption to ~550 nm. Such dopant-/additive- free TiO_2 assembly exhibits considerable photocatalytic activity under visible light due to its narrower bandgap than individual nanocrystals. Further, electron paramagnetic resonance measurement is used to confirm the capability of generating reactive $^{\bullet}OH$ radicals on the surface of assembled TiO_2 under visible-light irradiation.

Introduction

Semiconductor photocatalysts have attracted considerable interests in environmental purification, water splitting, and photoelectric conversion. The prime photocatalyst, TiO_2, remarkably is safe, abundant, inexpensive and stable.[1,2] However, the large bandgap (3.2 eV) of anatase TiO_2 seriously limits its use only to the UV region (about 3~5 % of solar spectrum), making it less applicable in industrial fields. To utilize a larger fraction of solar energy, many approaches have been conducted for narrowing the bandgap of TiO_2 so that the light absorption can be extended to visible region. The popular methods include doping with metal or nonmetal impurity and surface sensitization.[3-5] Although the attempts at enhancing visible light activity by doping have been proven successful, the impurities or dopant-induced defect states in the TiO_2 lattice may act as recombination centers for the photogenerated charge carriers. When the electrons and holes meet, they annihilate with the release of heat; sometimes the increased recombination negatively affects the photocatalytic activity.[6] For TiO_2 surface modification, the dye sensitizer additives will also become pollutants to environment and their photostability needs to be improved.[7] Therefore, a dopant-/additive- free method would be ideal for narrowing the bandgap of pure TiO_2 phase to match the visible light energy.

The high-pressure cubic TiO_2 phase has been reported that exhibits visible light absorption.[8,9] However, it is not stable at atmospheric pressure and not suitable for photocatalysis applications. Afterwards, Ariga et al reported the first example of visible light responsible photo-oxidation on TiO_2(001) surface.[10] It was revealed that the surface phases of pure TiO_2 with reduced bandgap might exist and be stable under ambient conditions.[10,11] Most recently, engineering the surface properties of TiO_2 was explored as a novel approach to offer hope that its efficiency can be increased within visible region.[12] Using repeated ion sputtering and vacuum annealing to ~650 °C, Batzill's group obtained rutile TiO_2(011) single crystals, cleaned the surface by argon ion irradiation, and annealed in a low pressure of oxygen. After treatment, the surface atoms had re-arranged themselves, showing a reduced bandgap of ~2.1 eV.[13] Mao's group introduced disorder in the surface layers of nanophase TiO_2 and produced black powders through hydrogenation. The highly defective amorphous layer caused about 2.18 eV up-shift of the valence band edge.[14] After that, the practice on altering the surface properties by hydrogenation has been applied to TiO_2 and other semiconductors for a wide range of applications.[15-21] Ye's group reduced the bandgap of anatase TiO_2 nanocrystals (NCs) to 2.8 eV by assembling individual NCs during evaporation of ethanol.[22] The key of preparing such individual NCs is to experience a microwave assisted solvothermal process in ethanol/benzyl alcohol mixture, so that they can possess high affinity with ethanol molecules to form Ti–Ti bonds at interfaces. As these recent works point out, surface engineering might be a valuable new approach to yielding pure TiO_2 phase with reduced bandgap. Although the above methods for narrowing the bandgap are relatively complicated, they give us some hints in designing a

facile strategy to alter the surface property of TiO_2 crystals for the same goal.

Using ethanol as the sole organic solvent, TiO_2 nanocrystals are synthesized and assembled together via a designed soft-chemical route, consisting of acid peptization and evaporation induced self-assembly (EISA) process. Such dopant-/additive-free TiO_2 assembly show a bright yellow colour with the onset of optical absorption extending to ~ 550 nm. In the photocatalytic reaction, the yellow assembled TiO_2 generates reactive oxygen species such as $^{\bullet}OH$ radicals and exhibits considerable photocatalytic activity on the decomposition of methylene blue under visible light irradiation.

Experimental Section

Materials Preparation

Step I: Synthesis of TiO_2 Hydrosol. TiO_2 nanoparticles in hydrosol were synthesized via a soft-chemical process based on the well-established method in our previous works.[23-25] In a typical synthesis, 3.00 mL titanium tetra-n-butoxide was mixed with 25.00 mL absolute ethanol, and then the solution was added into 30.00 mL double-distilled water drop by drop under vigorous stirring. After complete addition, the suspension was kept on stirring at 70 °C for about 50 min to ensure the complete hydrolysis and the concentration of solution. Subsequently, 70.00 mL 0.055 M HNO_3 was added and the mixture was continuously stirred at 70 °C for 4 h in airproof condition. Then the product was diluted with water to 100 mL for further use.

Step II: Synthesis of Assembled TiO_2 Flakes. A certain amount of TiO_2 hydrosol (20~30 mL) was highly concentrated by rotary evaporation to about 2 mL. Then, the sample was re-dispersed in absolute ethanol and concentrated by rotary evaporation again. After three cycles, most of water in the hydrosol was replaced by absolute ethanol. The followed assembly of individual TiO_2 nanoparticles was occurred during evaporation induced self-assembly (EISA) process. The concentrated TiO_2/ethanol colloid was diluted with absolute ethanol to 30 mL and stirred at 60 °C for 24 h in airproof condition. After that, the mixture was washed with absolute ethanol in an ultrasonic bath and purified by centrifugation for two times. Then the TiO_2 nanocrystals were diluted with absolute ethanol to 20 mL and transferred into a 50 mL beaker. Finally it was placed in a drying box at 70 °C for 72 h and at 100 °C for 3 h. In this way, the assembled TiO_2 flakes were obtained, which were labeled as A1, A2, A3 (Table 1). The crushed powder of A2 was labeled as A4 for comparison. The experimental parameters of sample A5 were similar to sample A2 except the drying time.

Characterization

Fourier-transform infrared (FT-IR) spectrum was recorded on a Nicolet Avatar 360 FT-IR Spectrometric Analyzer in the range of 400-4000 cm−1 with KBr pellet. Powder X-ray diffraction (XRD) patterns were obtained on an XRD-6000 X-ray diffractometer (Shimadazu Corporation, Japan) using graphite monochromatic copper radiation (Cu Kα) at 40 kV, 30 mA. The samples were scanned over the diffraction angle range (2θ) of 5–80°, which covers the main characteristic diffraction peaks of anatase TiO_2. UV-visible diffuse reflectance spectrum (UV-vis DRS) was measured on a TU 1901 UV–vis spectrophotometer (Puxi, Inc. Beijing) equipped with an integrating sphere attachment over a range of 250-550 nm. Transmission electron microscopy (TEM) and high resolution transmission electron microscopy (HRTEM) image of TiO_2 hydrosol were taken on a JEOL JEM 2010FEF (UHR) microscope operating at an accelerating voltage of 200 kV. Scanning electron microscope (SEM) measurements were carried out on a Hitachi S-4300 (Japan) microscope equipped with energy-dispersive X-ray spectroscopy (EDS). X-ray photoelectron spectroscopy (XPS) measurements were performed using a PHI5700 ESCA system (Physical Electronics) with an Mg Kα X-ray source. The binding energy shifts were corrected using the C 1s level at 284.6 eV as an internal standard, to compensate for the surface-charging effect during data analysis.

Photocatalytic Test

The photocatalytic activities of assembled TiO_2 flakes (A1-A3, A5), crushed powder (A4) and commercial TiO_2 materials (P25) were measured by degrading methylene blue (MB) under visible-light irradiation. In the test, a 50 mL beaker was filled with 10.00 mL aqueous solution of MB dye (40 μL of 0.2 wt%). The concentration of photocatalyst was 0.50 g/L and the starting pH value was adjusted to about 2.5. The mixture was kept under constant air-equilibrated conditions before and during the irradiation. Before irradiation, the suspensions were stirred for 40 min in the dark to establish adsorption–desorption equilibrium. A 300 W halogen lamp (Institute of Electric Light Source, Beijing) was used as visible-light source. A cutoff filter was settled to completely remove any radiation below 420 nm and to ensure illumination by visible-light. At given time intervals, the suspension was sampled and centrifuged for analysis by recording the dye absorption spectra using a TU 1900 UV–vis spectrophotometer (Puxi Inc., Beijing, China) equipped with 1 cm quartz cells. The changes in maximum absorption (664 nm) versus irradiation time ($C/C_0 \sim t$) were obtained, which could reflect the decrease in dye concentration.

Detection of $^{\bullet}OH$ Radicals in Photocatalytic System

A Brucker A200S spectrometer (Germany) was used to record the electron paramagnetic resonance (EPR) signals of $^{\bullet}OH$

Table 1 Experimental conditions as well as element compositions of as-prepared samples.

Sample	Ethanol treatment		Drying time at 100 °C	At%[b]		Atomic ratio of Ti:O
	volume of TiO_2 sol	volume of ethanol		O	Ti	
A1	20 ml	30 ml	3 h	52.11 %	47.89 %	1:1.09
A2	25 ml	30 ml	3 h	35.65 %	64.35 %	1:0.54
A3	30 ml	30 ml	3 h	49.53 %	50.47 %	1:0.98
A4[a]	25 ml	30 ml	3 h	69.52 %	30.48 %	1:2.28
A5	25 ml	30 ml	2 h	54.53 %	45.47 %	1:1.20

[a] A4 is the crushed powder of A2. [b] The values of At% are measured by energy-dispersive spectroscopy (EDS).

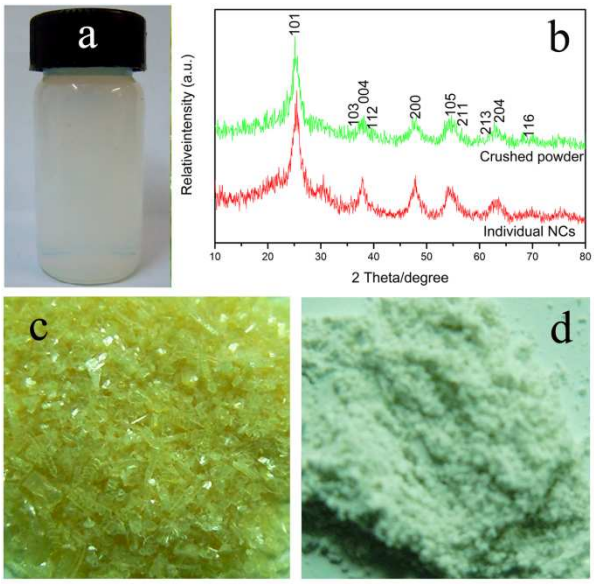

Fig. 1 (a) Photograph of TiO_2 NCs being re-dispersed in absolute ethanol; (b) XRD patterns of individual TiO_2 NCs directly dried from hydrosol and crushed powder from the assembled TiO_2 (sample A4); (c) Photograph of assembled TiO_2 flakes of sample A2; (d) Photograph of crushed TiO_2 powder from assembled flakes (sample A4).

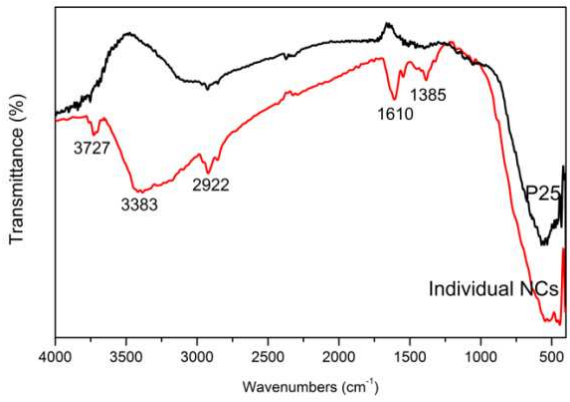

Fig. 2 FTIR spectra of P25 and individual TiO_2 NCs from a direct peptization process. The hydrosol sample was treated with sedimentation, centrifugation, and vacuum drying at 40 °C for 8 h and was milled into tiny powders for measurements.

radicals spin-trapped by 5,5-dimethyl-1-pyrroline N-oxide (DMPO) after visible-light illumination of the suspensions of assembled TiO_2 flakes at ambient temperature. The parameters for the EPR measurements were centre field, 3511.940 G; microwave frequency, 9.860 GHz; and power, 2.259 mW.

Results and discussion

Structural Characterization

TiO_2 NCs that were synthesized from soft-chemical system could be easily dispersed in water to form stable hydrosol. Then the hydrosol was highly concentrated by rotary evaporation and re-dispersed in absolute ethanol. After three cycles, most of water was replaced by ethanol. As shown in Fig. 1a, the resulted mixture still appeared to be stable colloid and no sedimentation occurred, indicating the high affinity between TiO_2 NCs and ethanol molecules. According to XRD analysis (Fig. 1b), both individual NCs and crushed powder of assembled TiO_2 are in anatase phase (JCPDS No. 12-1272). Although the assembling process endows TiO_2 NCs different appearance (Fig. 1c and d), it does not alter the crystal phase.

The FTIR spectrum was used to study the surface functional groups of powders from as-synthesized hydrosol sample (Fig. 2). The strong and broad peak at 400-1000 cm^{-1} is characteristic of the Ti-O lattice vibration in TiO_2 crystals. The 1385 cm^{-1} absorption corresponds to the C-O stretching in residual terminal titanium alkoxide ($-OC_4H_9$), while the band at 2922 cm^{-1} is due to C-H stretching vibration from alkyl groups bound to the surface of TiO_2 particles during the hydrolysis process. It has been revealed that there are two types of OH groups (t and b) occurring on the surface of TiO_2 NCs in low-temperature-prepared hydrosol, where the designations "t" and "b" refer to terminal hydroxyl (bound to one Ti^{4+} cation) and bridging hydroxyl (bound to two Ti^{4+} cations), respectively.[26] The O-H stretching of OH (b) usually appears at ~3667 cm^{-1}, which is interfered with that of adsorbed water.[27] The peak at 1610 cm^{-1} is the typical bending mode of adsorbed water molecule.[28] From the wide absorption band at 3000-3700 cm^{-1}, it is hard to tell the difference in surface OH (b) between the two samples. But the significant and convincing information is that the O-H stretching of OH (t) is observed only in the as-synthesized sample, which displays distinct band at 3727 cm^{-1}.[29] The results implied that abundant hydroxyl on the surface of TiO_2 NCs in hydrosol system might be the reason of relatively high affinity with water or ethanol as dispersion medium, resulting in the formation of stable colloid. Such affinity between TiO_2 NCs and ethanol molecules will facilitate the individual NCs to assemble together by interfacial

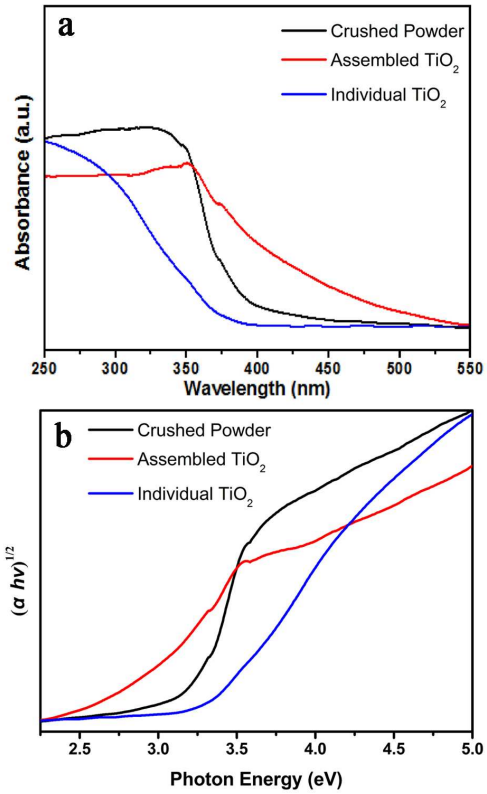

Fig. 3 (a) UV-vis absorption spectra; (b) corresponding plots of $(\alpha h\nu)^{1/2}$ as a function of photon energy.

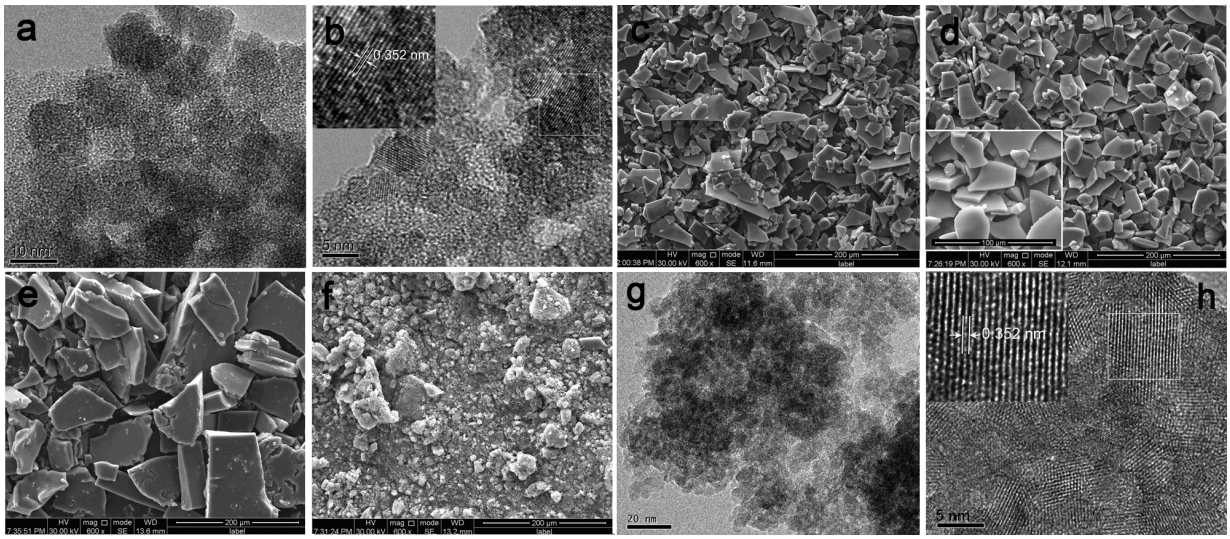

Fig. 4 TEM (a) and HRTEM (b) images of individual TiO_2 NCs in hydrosol. SEM images of assembled TiO_2 NCs in sample A1 (c), A2 (d), A3 (e), and the crushed powder A4 (f). TEM (g) and HRTEM (h) images of the crushed powder A4. The inserts in (b), (d), and (h) are the high-magnified TEM images and SEM image, respectively.

Ti–Ti electronic bonding during evaporation induced self-assembly (EISA) process. The newly formed TiO_2 NC assemblies show bright yellow colour after being treated with ethanol (Fig. 1c), which is different from white individual NCs. When crushing the yellow assemblies into powders, the colour changed to white again (Fig. 1d). As shown in UV-vis absorption spectra, the absorption edge of the assembled TiO_2 NCs is red shifted to 550 nm in comparison to individual ones (Fig. 3a). After converting to photon energy spectra (Fig. 3b), the difference in bandgap can be clearly observed. The bandgap of newly formed NC assemblies is about 2.7 eV (459 nm), while that of crushed and individual NCs is 3.2 eV (388 nm) and 3.3 eV (376 nm), respectively. The changes in bandgap values suggest that the interfacial bonding in yellow assemblies is the reason of bandgap narrowing and can be destroyed by crushing.

TEM observations in Fig. 4a show the high dispersion as well as high uniformity of individual anatase NCs with a small size of 5~8 nm, appearing a strong attractive force between them. The insert in HRTEM image showed the lattice spacing of 0.352 nm, which were the identifications of the crystallographic spacing of anatase TiO_2 (Fig. 4b). Fig. 4c-4f shows the SEM images of assembled samples A1-A4. The experimental conditions as well as the element compositions of these samples are given in Table 1. After treating with ethanol during EISA process, these individual TiO_2 NCs assembled together by interfacial Ti–Ti electronic bonding to form larger flakes. The size and uniformity of such flake-shaped assemblies can be controlled by varying the concentration of TiO_2 NCs in ethanol medium. At lower concentration, the individual NCs could not fully aggregate and assemble together, resulting in the existence of many scattered fragments (Fig. 4c). When increasing the concentration, the assemblies become more uniform with an average size of 20~50 μm (Fig. 4d), which is much smaller and thinner than the crystals prepared by microwave assisted solvothermal process in ethanol/benzyl alcohol (about several hundred micrometers).[22] The further increase of concentration will increase the packing degree of assemblies so that larger and thicker bulks generated from the system (Fig. 4e). As shown in Fig. 4f, the flake-shaped assemblies are destroyed after being crushed into powders. Fig. 4g and 4h display the obvious aggregations of TiO_2 NCs with no change of lattice structure after crushing.

The corresponding EDS spectra and the element compositions of Fig. 4c-4f were given in Fig. 5. The surfaces of assembled TiO_2 flakes (A1-A3) accommodate stoichiometrically excessive amounts of titanium, while the atomic ratio of Ti to O in the crushed powder (A4) is almost stoichiometric (1:2.28). XPS analysis of Ti2p indicates that the assembly shows wider peaks with positive shift in comparison to crushed powder, as shown in Fig. 6a and Table S1 (Supporting Information). Gaussian fitting resolved both $Ti2p_{1/2}$ and $Ti2p_{3/2}$ peaks as doublets (Fig. 6b). One peak is the Ti^{4+} in crystal lattice of NCs and the other is Ti^{4+} from interfacial bonding. Gaussian fitted O1s XPS peaks show that the $^{*}O1s_{1/2}$ signal of the crushed powder is much stronger than that of assembly (Fig. 6c and d), implying the amount of adsorbed oxygen species increased after the destruction of interfacial bonding. The isolated TiO_2 NCs are surrounded by many nonbonding Ti 3d electrons.[30] These nonbonding Ti 3d state

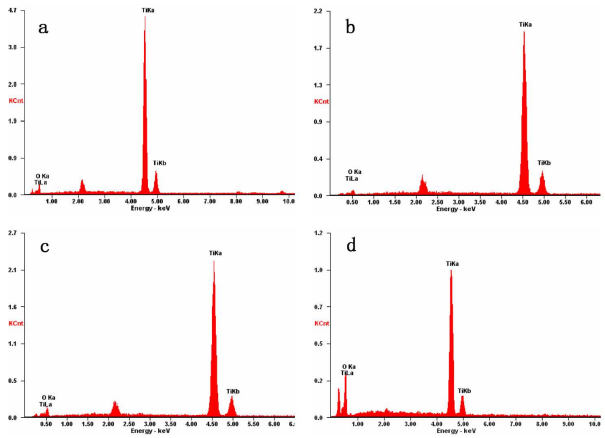

Fig. 5 EDS spectra of assembled TiO_2 NCs in sample A1 (a), A2 (b), A3 (c), and the crushed powder A4 (d).

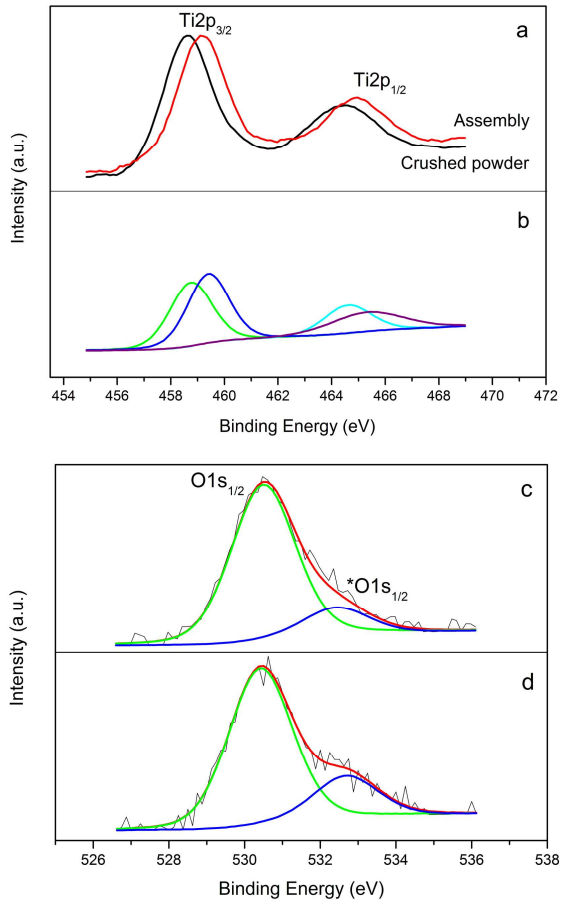

Fig. 6 XPS spectra of assembly and crushed powder. (a) High-resolution XPS spectra of Ti, (b) Gaussian fitting of $Ti2p_{1/2}$ and $Ti2p_{3/2}$ peaks in assembly, (c) high-resolution XPS spectrum and Gaussian fitting of O1s in assembly, (d) high-resolution XPS spectrum and Gaussian fitting of O1s in crushed powder.

forms the conduction band minimum (CBM) of TiO_2.[31,32] During EISA process, these excessive Ti will combine their wave functions and form a bond between the two adjacent NCs to generate large assemblies. As explained by Ye's group, oxygen vacancies are likely to form at the interface because their formation energy (4.18 eV) is much lower than that at the surface (4.62 eV). Ti–Ti bonds formed at the interface are a major characteristic of such defect levels, which located near the CBM.[22] Therefore, surface contacts of TiO_2 NCs should promote the formation of oxygen vacancy and Ti–Ti bonds at interfaces, resulting in the narrowed bandgap and visible light absorption.

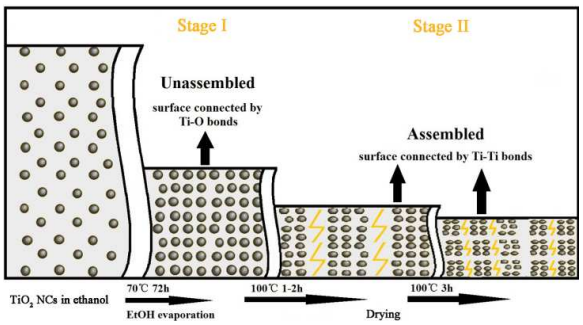

Scheme S1 Scheme representing the stages of assembled TiO_2 formation during EISA process.

Formation Mechanism of Assembled TiO_2

EISA process was first introduced by Brinker's group to prepare mesoporous silica films.[33,34] Then it was extended to the production of transition metal oxide and carbon materials with porous, multidimensional, or nanocomposite structure.[35-40] The evolution of TiO_2 NCs during the evaporation process is explained in Scheme 1, according to the EISA mechanism proposed by Sanchez's group.[41]

At stage I, the ethanol outside of TiO_2 NCs was evaporated and the inner ethanol between them left when evaporating at 70 °C for 72 h. Because of solvent shrinking, the highly dispersed NCs began to connect each other. At stage II, the inner ethanol was gradually evaporated when heated to 100 °C, which brought about the close surface contact of individual NCs. When sampling at drying time of 2 h (A5), the assembling proceeded inadequately so that many discrete particles were observed in large block (Fig. S1). These particles were surrounded by the residual ethanol molecules, which hindered the sufficient surface connection among them. After complete departure of ethanol vapor (drying for >3 h), the NCs assembled together with the formation of interfacial Ti-Ti bonding and oxygen vacancy. Meanwhile, the assembly split from the large block to produce uniform flakes.

Photocatalytic Test

The effect of surface engineering of TiO_2 NCs by EISA process on the photocatalytic activity under visible light irradiation is evaluated using methylene blue (MB) as model molecule. Although some organic dyes could be degraded by TiO_2 based on visible-light driven dye-sensitized mechanism,[42,43] it was reported that such dye-sensitized process for photodegradation of MB dye over common TiO_2 was unconspicuous under visible-light.[44] As expected, the negligible degradation of MB over commercial P25 and crushed powder is observed since their wide bandgap values do not permit them to be excited by visible light irradiation. However, the assembled samples all exhibit the capability of decomposing MB under visible irradiation (Fig. 7 and Fig. S2). A2 shows superior photodegradation rate to A1, A3, and A5, which may be attributed to the uniform and small size of assemblies. The photocatalytic stability is a problem for the assembled TiO_2, which is also stressed by Ye's group.[22] The yellow flakes will gradually turn white (several days) in aqueous solution or slowly turn white (several weeks) in air at room temperature. In the second cycle degradation of MB dye, the catalyst turns white with photoactivity decreasing to only 38% of the initial value (Fig. S3). After re-treating at 100 °C for 3 h, the colour turns yellow again and the photocatalytic activity of the recovered yellow assembly is about 64% of the first cycle. The colour change possibly comes from the external oxygen being incorporated into the assemblies and then destroying the interfacial Ti-Ti bonding in the assembly structure. Thus, the stability of the yellow TiO_2 flakes may be improved if preventing their exposure to oxygen-containing environment.

It is well-known that the photodegradation of organic molecules over pure TiO_2 is attributed to the reactive oxygen species (ROS) induced chain reaction under UV-light irradiation. EPR/DMPO measurement is carried out to detect the reactive $^{\bullet}OH$ radicals to confirm the capability of generating ROS on the

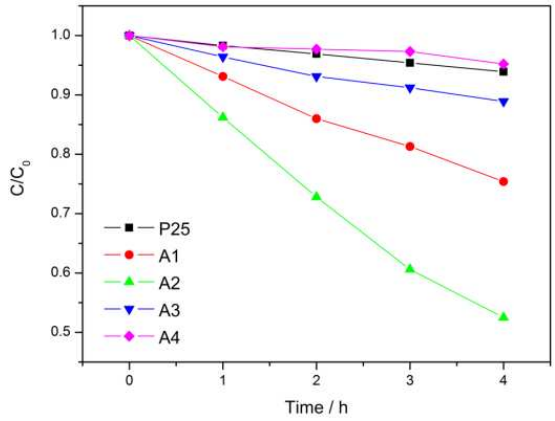

Fig. 7 Comparison of photocatalytic activities of the samples under visible light irradiation (300 W halogen lamp, λ > 420 nm). MB is used as the model with detection of the reduction of its absorption at 664 nm.

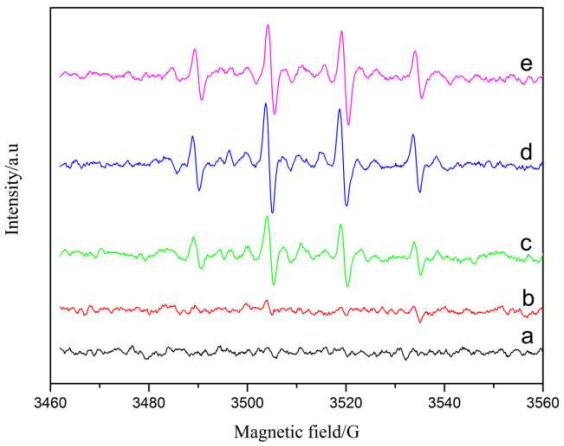

Fig. 8 The signal of DMPO-•OH adduct in the photocatalytic system for the EPR experiment. (a) dark; (b) 90 s visible-light illumination of crushed powder A4 suspension; (c) 30 s, (d) 60 s, and (e) 90 s visible-light illumination of assembled TiO_2 A2 suspension.

surface of assembled TiO_2 NCs under visible-light similar to common photocatalytic process. As shown in Fig. 8, no obvious signal is detected in the darkness as well as in the visible-light irradiation system containing crushed powder. For TiO_2 assemblies, the spectra are composed of quartet lines with a peak height ratio of 1:2:2:1 and the parameters are hyperfine coupling constants $a_N = a_H = 1.49$ mT after excitation by visible light. These parameters in the spectra are characteristic of the •OH spin adduct of DMPO.[45] The intensity of DMPO-•OH signal increases in the first 60 s of irradiation and decays subsequently. The EPR results suggest that the bandgap of TiO_2 assemblies is narrowed and visible light can excite them to produce ROS to participate in the photocatalytic reaction.

Conclusions

In summary, this work presents a dopant-/additive- free method for narrowing TiO_2 bandgap by surface engineering. Individual anatase TiO_2 NCs are synthesized and assembled together via a facile soft-chemical route using ethanol as the sole organic solvent. The high affinity between TiO_2 NCs and ethanol molecules is necessary for the formation of yellow flake-like assembly. The uniform assembly with an average size of 20~50 μm can be obtained by controlling the concentration of NCs in ethanol medium as well as the drying time during EISA process. In contrast to the crushed powder, the surfaces of assembled TiO_2 flakes accommodate stoichiometrically excessive amounts of Ti atoms. These excessive Ti atoms are inclined to combine their wave functions and form interfacial Ti-Ti bonds between the two adjacent NCs to generate larger assemblies. Replacing O atom by Ti will change the surface structural unit and the electronic structure, resulting in the light absorption of assembled TiO_2 extending to ~550 nm. Consequently, significant decomposition of MB dye is achieved in the photocatalytic system containing the yellow flake-like assembly under visible-light irradiation. The degradation mechanism involves the direct excitation of photocatalyst itself and the followed ROS induced chain reaction, similar to that of common TiO_2 irradiated by UV-light. We can envision such interfacial assembling strategy as a facile approach for altering the bandgap of semiconductor, which is valuable in designing visible light responsive materials for wide application in harvesting solar energy.

Acknowledgements

We thank the Analysis and Testing Center, Huazhong University of Science and Technology for their assistance in characterization of materials. This work is supported by the National Natural Science Foundation of China (21001037 and 21473064), the Special Fund of Harbin Technological Innovation talent (2013RFLXJ011), and the Research Fund for Talent Introduction of Huazhong University of Science and Technology (2014036).

Notes and references

[a] *Key Laboratory for Large-Format Battery Materials and System (Ministry of Education), School of Chemistry and Chemical Engineering, Huazhong University of Science and Technology, Wuhan 430074, China. E-mail: jingyu.wang@163.com; taoli@hust.edu.cn.*
[b] *Department of Chemistry, Harbin Institute of Technology, Harbin 150001, China.*
[c] *School of Chemistry and Environmental Engineering, Wuhan Institute of Technology, Wuhan 430074, China.*

† Electronic Supplementary Information (ESI) available: SEM images and photoactivity of sample A5, binding energy values of assembly and crushed powder from XPS results. See DOI: 10.1039/b000000x/

1 H. H. Chen, C. E. Nanayakkara and V. H. Grassian, *Chem. Rev.*, 2012, **112**, 5919–5948.
2 X. J. Lang, X. D. Chen and J. C. Zhao, *Chem. Soc. Rev.*, 2014, **43**, 473–486.
3 M. Yang, D. Kim, H. Jha, K. Lee, J. Paul and P. Schmuki, *Chem. Commun.*, 2011, **47**, 2032–2034.
4 R. Asahi, T. Morikawa, T. Ohwaki, K. Aoki and Y. Taga, *Science*, 2001, **293**, 269–271.
5 Y. C. Qiu, W. Chen and S. H. Yang, *Angew. Chem. Int. Ed.*, 2010, **49**, 3675–3679.
6 W. Choi, A. Termin and M. R. Hoffmann, *J. Phys. Chem.*, 1994, **98,** 13669–13679.
7 P. T. Nguyen, A. R. Andersen, E. M. Skou and T. Lund, *Sol. Energy Mater. Sol. Cells*, 2010, **94**, 1582–1590.
8 D. Y. Kim, J. S. de Almeida, L. Koci and R. Ahuja, *Appl. Phys. Lett.*, 2007, **90**, 171903(1–3).
9 M. Mattesini, J. S. de Almeida, L. Dubrovinsky, N. Dubrovinskaia, B. Johansson and R. Ahuja, *Phys. Rev. B*, 2004, **70**, 115101(1–9).
10 H. Ariga, T. Taniike, H. Morikawa, M. Tada, B. K. Min, K. Watanabe, Y. Matsumoto, S. Ikeda, K. Saiki and Y. Iwasawa, *J. Am. Chem. Soc.*, 2009, **131**, 14670–14672.

11 A. C. Papageorgiou, N. S. Beglitis, C. L. Pang, G. Teobaldi, G.; Chen, Q. Cabailh, A. J. Fisher, W. A. Hofer and G. Thornton, *Proc. Natl. Acad. Sci. U. S. A.*, 2010, **107**, 2391–2396.

12 U. Diebold, *Nat. Chem.*, 2011, **3**, 271–272.

13 J. G. Tao, T. Luttrell and M. Batzill, *Nat. Chem.*, 2011, **3**, 296–300.

14 X. Chen, L. Liu, P. Y. Yu and S. S. Mao, *Science*, 2011, ***331***, 746–750.

15 X. H. Lu, G. M. Wang, T. Zhai, M. H. Yu, J. Y. Gan, Y. X. Tong and Y. Li, *Nano Lett.*, 2012, **12**, 1690–1696.

16 X. H. Lu, G. M. Wang, S. L. Xie, J. Y. Shi, W. Li, Y. X. Tong and Y. Li, *Chem. Commun.*, 2012, **48**, 7717–7719.

17 J. Y. Shin, J. H. Joo, D. Samuelis and J. Maier, *Chem. Mater.*, 2012, **24**, 543–551.

18 T. Leshuk, R. Parviz, P. Everett, H. Krishnakumar, R. A. Varin and F. Gu, *ACS Appl. Mater. Interfaces*, 2013, **5**, 1892–1895.

19 X. Yu, B. Kim and Y. K. Kim, *ACS Catalysis*, 2013, **3**, 2479–2486.

20 S. Li, J. X. Qiu, M. Ling, F. Peng, B. Wood and S. Q. Zhang, *ACS Appl. Mater. Interfaces*, 2013, **5**, 11129–11135.

21 Y. M. Zhu, D. S. Liu and M. Meng, *Chem. Commun.*, 2014, **50**, 6049–6051.

22 H. Tong, N. Umezawa and J. H. Ye, *Chem. Commun.*, 2011, **47**, 4219–4221.

23 D. Su, J. Y. Wang, Y. P. Tang, C. Liu, L. F. Liu and X. J. Han, *Chem. Commun.*, 2011, **47**, 4231–4233.

24 L.A. Gu, J.Y. Wang, Z.J. Zou and X.J. Han, *J. Hazard. Mater.*, 2014, **268**, 216–223.

25 L.Y Hu, J.Y. Wang, J.X. Zhang, Q.Y. Zhang and Z.H. Liu, *RSC Adv.*, 2014, **4**, 420–427.

26 M. A. Henderson, *Langmuir*, 1996, **12**, 5093–5098.

27 J. R. S. Brownson, M. I. Tejedor-Tejedor and M. A. Anderson, *J. Phys. Chem. B*, 2006, **110**, 12494–12499.

28 C. Deng, P. F. James and P. V. Wright, *J. Mater. Chem.*, 1998, **8**, 153–159.

29 J.Y. Wang, Z.H. Liu and R.X. Cai, *Environ. Sci. Technol.*, 2008, **42**, 5759–5764.

30 A. L. Linsebigler, G. Q. Lu and J. T. Yates, *Chem. Rev.*, 1995, **95**, 735–758.

31 W. J. Yin, S. H. Wei, M. M. Al-Jassim and Y. F. Yan, *Appl. Phys. Lett.*, 2011, **99**, 142109(1–3).

32 B. J. Morgan and G. W. Watson,. *Phys. Rev. Lett.*, 2010, **82**, 144119(1–11).

33 Y. F. Lu, R. Ganguli, C. A. Drewien, M. T. Anderson, C. J. Brinker, W. L. Gong, Y. X. Guo, H. Soyez, B. Dunn, M. H. Huang and J. I. Zink, *Nature*, 1997, **389**, 364–368.

34 C. J. Brinker, Y. F. Lu, A. Sellinger and H. Y. Fan, *Adv. Mater*., 1999, **11**, 579–585.

35 C. M. Ghimbeu, M. Soprony, F. Sima, C. Vaulot, L. Vidal, J.-M. L. Meins and L. Delmotte, *RSC Adv.*, 2015, **5**, 2861-2868.

36 J. M. Szeifert, J. M. Feckl, D. Fattakhova-Rohlfing, Y. J. Liu, V. Kalousek, J. Rathousky and T. Bein, *J. Am. Chem. Soc.*, 2010, **132**, 12605–12611.

37 W. Q. Cai, J. G. Yu, C. Anand, A. Vinu and M. Jaroniec, *Chem. Mater*., 2011, **23**, 1147–1157.

38 L. Luo, P. P. Wang, D. W. Jing and X. Wang, *CrystEngComm*, 2014, **16**, 1584-1591.

39 A. Wolosiuk, N. G. Tognalli, E. D. Martinez, M. Granada, M. C. Fuertes, H. Troiani, S. A. Bilmes, A. Fainstein and G. J. A. A. Soler-Illia, *ACS Appl. Mater. Interfaces*, 2014, **6**, 5263–5272.

40 S. Semlali, T. Pigot, D. Flahaut, J. Allouche, S. Lacombe and L. Nicole, *Appl. Catal. B*, 2014, **150**, 656–662.

41 E. L. Crepaldi, G. J. D. A. Soler-Illia, D. Grosso, F. Cagnol, F. Ribot and C. Sanchez, *J. Am. Chem. Soc.*, 2003, **125**, 9770–9786.

42 G. Liu, T. Wu, J. Zhao, H. Hidaka and N. Serpone, *Environ. Sci. Technol.*, 1999, **33**, 2081–2087.

43 Y. M. Xu and C. H. Langford, *Langmuir*, 2001, **17**, 897–902.

44 J. W. Tang, Z. G. Zou, J. Yin and J. H. Ye, *Chem. Phys. Lett.*, 2003, **382**, 175–179.

45 S. K. Han, S. N. Nam and J. W. Kang, *Water Sci. Technol.*, 2002, **46**, 7–12.

Table of contents

Using a green interfacial assembling strategy, the dopant-/additive- free TiO_2 assembly exhibits considerable visible photoactivity due to its narrowed bandgap.